Medical Engineering and Physics 70 (2019) 29–38

Contents lists available at ScienceDirect

Medical Engineering and Physics

journal homepage: www.elsevier.com/locate/medengphy

Catheter thermal energy generation and temperature in rotational atherectomy

Yao Liu[a,b,*], Yang Liu[b], Yihao Zheng[c], Beizhi Li[b], Albert Shih[b]

[a] Mechanical Engineering, North University of China, Shanxi, China
[b] Mechanical Engineering, University of Michigan, Ann Arbor, Michigan, USA
[c] Mechanical Engineering, Worcester Polytechnic Institute, Worcester, MA, USA

ARTICLE INFO

Article history:
Received 7 July 2018
Revised 31 March 2019
Accepted 9 June 2019

Keywords:
Rotational atherectomy
Thermal model
Saline temperature

ABSTRACT

This research studies the catheter friction thermal energy generation and saline temperature in rotational atherectomy (RA). RA is a catheter-based procedure utilizing a high-speed (typically 130,000 to 210,000 rpm) miniature grinding wheel to remove hardened calcified plaque inside the artery to restore the blood flow. During RA, elevated temperature due to the friction within the catheter may lead to complications such as slow-flow/no-reflow and myocardial infarction. RA experiments were conducted to measure the catheter temperature. An advection-diffusion model with inverse heat transfer solution was developed to estimate the spatial and temporal distributions of saline temperature and study effects of the rotational speed, catheter insertion length, and flow rates of blood-mimicking water and saline. The saline temperature rise is higher with higher wheel rotational speed, shorter insertion length, and lower flow rates of blood-mimicking water and saline. The wheel rotational speed and blood flow rate are the two most significant parameters affecting the saline and blood-mimicking water mixture temperature, which exhibits the highest (9 °C) rise under the 175,000 rpm wheel rotational speed and no blood-mimicking water flow (totally occluded artery) condition. This research provides insights and guidelines on RA device and clinical procedure from the thermal perspective.

1. Introduction

Rotational atherectomy (RA) is an interventional cardiology procedure to remove the plaque inside the artery. RA is currently used in 3% to 5% of percutaneous coronary interventions [1], particularly for the calcified (and hardened) plaque, arterial bifurcation, ostial stenosis, and in-stent restenosis [2], but with high complication rates. The catheter, as shown in Figure 1, is assembly of the sheath, drive shaft, guidewire, and grinding wheel. The high-speed metal bond diamond grinding wheel can pulverize the plaque to small particles (absorbed by the blood) in RA. Clinically, the RA grinding wheel with a diameter ranging from 1.25 to 2.5 mm is driven by a drive shaft rotating at 130,000 to 210,000 rpm [3]. A stationary guidewire is inside the drive shaft and grinding wheel to guide the rotation and translational advancement of the wheel through the artery for grinding the plaque. A stationary sheath outside the drive shaft prevents the high-speed rotating shaft from contacting the arterial wall. Blood flows outside the sheath. Inside the sheath, saline flows for cooling and hydrodynamic lubrication of the high speed rotating drive shaft.

Heat is generated inside the sheath during RA due to the friction between the high-speed rotational drive shaft and the stationary guidewire and sheath. The heat is carried away by the saline and transferred through the sheath wall to the blood. The saline with elevated temperature is mixed with the blood at the exit of the sheath, and increased the temperature of the mixture of saline and blood (Fig. 1). Elevated blood temperature above 42 to 43 °C [4–6] may cause blood cell coagulation and result in the vessel blockage and other complications. Clinical studies showed 1.2 to 7.6% slow-flow/no-reflow and 1.2 to 4.5% myocardial infarction complication rates in RA [1,7,8]. Both complications are related to the elevated blood temperature in RA.

The elevated temperature of plaque in RA has been investigated. An early study utilizing the infrared thermal imaging to measure the temperature of ex-vivo vascular tissue showed that RA was capable of generating significant heat and potential thermal tissue damage [9]. Reisman et al. [10] studied the effect of slow and aggressive advancements of the wheel on temperature measured using a thermocouple embedded in the bone surrogate (representing the calcified plaque). For slow advancement, the temperature rise at 0.5 mm under the bone surface was 2.6 ± 1.3 °C, which is

* Corresponding author at: Mechanical Engineering, North University of China, Shanxi, China.
E-mail address: liuyao@nuc.edu.cn (Y. Liu).

https://doi.org/10.1016/j.medengphy.2019.06.014
1350-4533/

Nomenclature

A_n	Constant in saline thermal model
b	Constant in saline thermal model
c	Specific heat of saline, J/(kg·K)
c_s	Specific heat of sheath, J/(kg·K)
D_i	Inner diameter of the sheath, mm
D_o	Outer diameter of the sheath, mm
DOF	Degree of freedom
E	Sum of squared errors between T_{saline} and T_{saline_TC}, °C^2
E_s	Sum of squared errors between T_{sheath} and T_{sheath_exp}, °C^2
g	Constant in saline thermal model
H	$= 4h/(\rho c D_o)$, s^{-1}
h	Convective heat transfer coefficient between saline and sheath, W/(m^2·K)
h_s	Convective heat transfer coefficient between water and sheath, W/(m^2·K)
K	$=k/(\rho c)$, m^2/s
k	Thermal conductivity of saline, W/(m^2·K)
k_s	Thermal conductivity of sheath, W/(m^2·K)
L_E	Distance from the starting point to the ending point of catheter, m
L_I	Distance from the starting point to the insertion point of catheter, m
L_{TE}	Thermal entrance length for the saline flow, m
l	Insertion length
n	= 1, 2, 3, …
Pr	Prantdl number of water, =6.62
Re	Reynolds number of the saline flow
Q	$= q/(\rho c)$, °C/s
Q_s	Saline flow rate, ml/min
Q_b	Blood-mimicking water flow rate, ml/min
q	Friction thermal energy generation rate per unit volume, W/m^3
q_1, q_2, q_3, q_4	Heat flux on the boundaries of a control volume of sheath, W/m^2
T_I	Measured temperature of sheath at the insertion point of catheter, °C
T_E	Measured temperature of sheath at the ending point of catheter, °C
T_o	Initial temperature of saline and sheath, °C
T_{saline}	Model predicted temperature of saline, °C
T_{saline_exp}	Measured temperature of saline at TC8, °C
T_{saline_TC}	Temperature of saline at TC1-TC7 thermocouple locations in the model, °C
T_{sheath}	Model predicted temperature of sheath, °C
T_{sheath_exp}	Measured temperature of sheath, °C
$\bar{T}_{sheath\_exp}$	Mean of measured temperature of the sheath, °C
T_∞	Temperature of the blood mimicking water, °C
t	RA process time, s
v	Velocity vector of saline flow, m/s
v_z	Speed of saline flow, m/s
z	Distance from the starting point of the catheter along its length, m
ΔT	Model predicted temperature rise of saline at TC8, °C
ΔT_{exp}	Measured temperature rise of saline at TC8, °C
ΔT_s	Model predicted temperature rise of sheath, °C
ΔT_{s_exp}	Measured temperature rise of sheath, °C
δ	Threshold for convergence
ρ	Density of saline, kg/m^3
ρ_s	Density of sheath, kg/m^3
φ_n	Constant in saline thermal model
ω	Rotational speed, rpm
$()^{(i)}$	ith iteration
$^j()$	jth thermocouple
λ	Constant in saline thermal model

lower than the 13.9 ± 1.0 °C measured using the fast and aggressive wheel advancement. A recent study of the thermal energy generation rate in RA utilizing the inverse heat transfer and embedded thermocouples in the bone surrogate confirmed a minimal thermal energy generation on the bone surrogate with slow advancement of the wheel and the elevated temperature of the saline is due to the friction of the high-speed rotating drive shaft with the stationary guidewire and sheath [11]. Our review indicates that there is a lack of research on catheter and saline temperatures in RA. The goal of this study is to identify the catheter friction thermal energy generation and establish a thermal model to predict the saline temperature in RA.

Both experimental and thermal modeling studies are conducted in this study. Experiments based on the clinical RA device and procedure have been set up to measure temperatures of the sheath and mixture of the saline and blood-mimicking water at the sheath outlet. To embed a micro thermocouple tip in the thin (0.2 mm) sheath wall for direct saline temperature measurement is difficult. The advection-diffusion thermal model and inverse heat transfer solution [12] are established to solve the spatial and temporal temperature distributions of the saline. The model predicted saline temperatures are compared with the experimental measurements, which are within 0.6 °C at all rotational speeds and blood flow conditions. Results show that the wheel rotational speed and blood flow rate are the two most significant parameters affecting the saline and blood-mimicking water mixture temperature which exhibits the highest (9 °C) rise under the 175,000 rpm wheel rotational speed and no blood-mimicking water flow (totally occluded artery) condition.

2. Experimental setup

Figure 2(a) shows the experimental setup which consists of three key modules: 1) RA device, 2) fluid delivery system, and 3) temperature measurement.

2.1. RA device

The RA device, Rotablator™ by Boston Scientific, includes a pressure regulator, an air turbine, and a catheter, as shown in

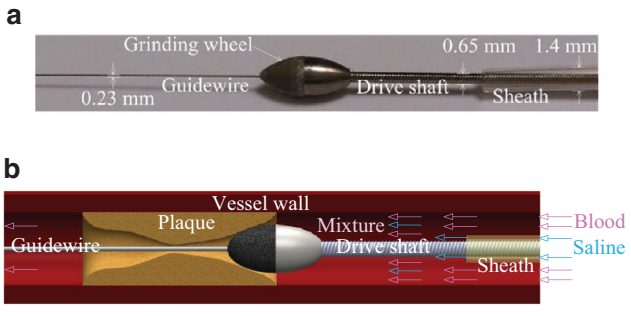

Figure 1. RA for plaque grinding: (a) catheter, including sheath, drive shaft, guidewire, and grinding wheel and (b) overview of the procedure.

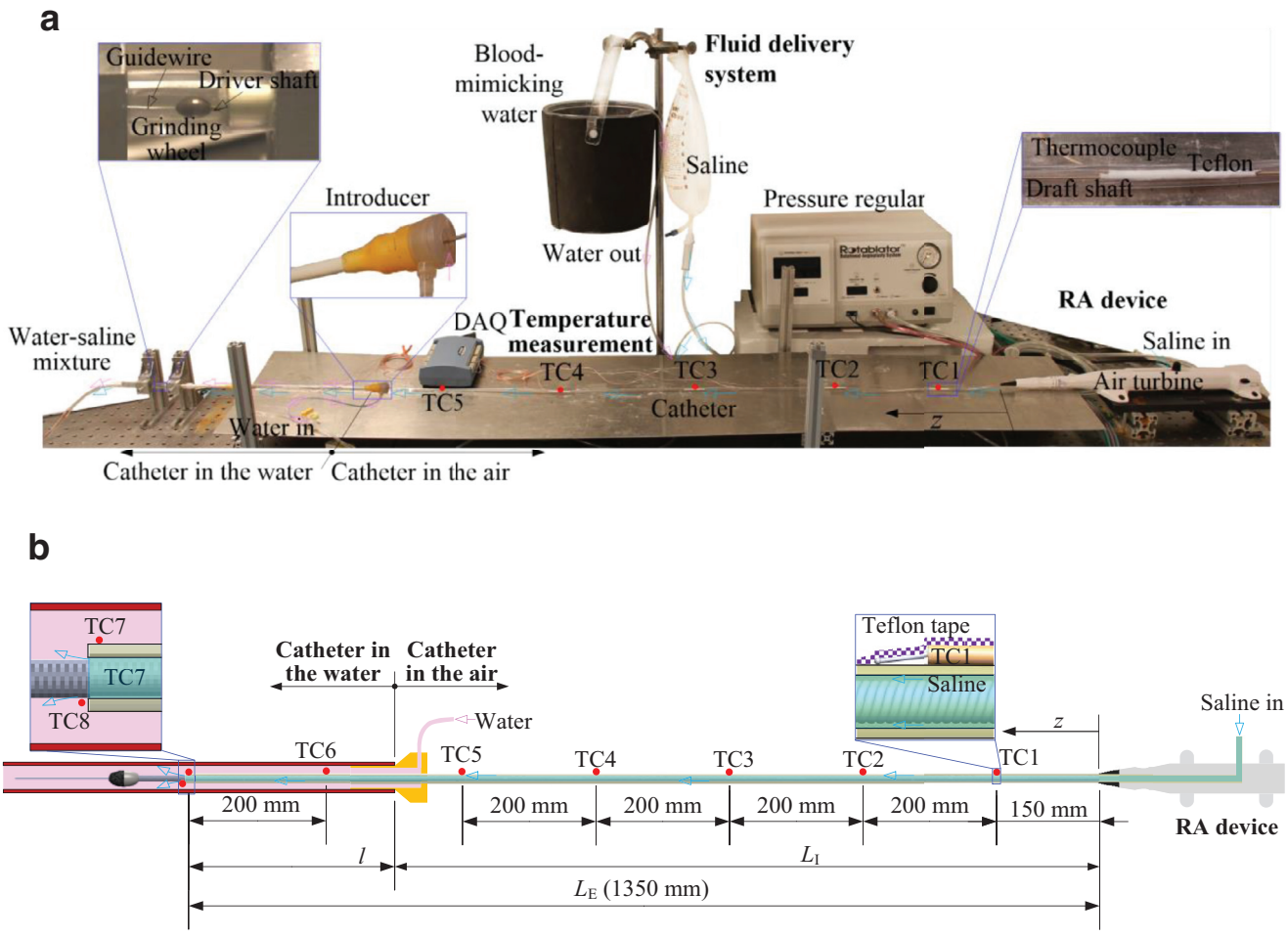

Figure 2. (a) Experimental setup with RA device, fluid delivery system, and temperature measurement and (b) schematic of setup and thermocouple location.

Figure 2(a). The pressure regulator controls the compressed air flow to drive the air turbine at 135,000, 155,000, and 175,000 rpm in this study. The grinding wheel is driven by a drive shaft (connected to the air turbine) inside the catheter. The cross-section of catheter, as illustrated in A-A in Figure 3(a), consists of a stainless steel guidewire (0.23 mm diameter), a drive shaft (0.65 mm outer diameter and 0.29 mm inner diameter), and a sheath (outer diameter $D_o = 1.4$ mm and inner diameter $D_i = 1$ mm). The drive shaft is made of three helically winded stainless steel coils (0.18 mm diameter) with a length of 1350 mm.

Saline flows inside the sheath. The frictional heat is transported to the saline inside the sheath. The heat in saline with elevated temperature is transferred through the thin (0.2 mm) sheath wall to the surrounding air (before the sheath entered the introducer in Fig. 2) or to the blood-mimicking water (after the sheath entered the introducer).

2.2. Fluid delivery system

Blood-mimicking water and saline were two types of fluid in RA experiments. The blood-mimicking water was filtered using the EMD Milli-Q system (Merck KGaA, Darmstadt, Germany) before the experiment. In the experiment, the room temperature blood-mimicking water, marked by the pink arrow in Figure 2(a), passed from the reservoir via the introducer, which works as a hemostasis valve, to a 6 mm inner diameter PVC tube, which mimics the blood vessel. The flow rate of blood-mimicking water is Q_b, a variable in this study.

The saline, a solution of 0.90 wt% of NaCl, passed through the air turbine unit into the catheter, as shown in Figure 2(a). The flow rate of saline is Q_s, which is another variable in this study. The catheter was inserted into the PVC tube via the introducer. As shown in Figs. 2(b) and 3(b), the sheath was surrounded by air before and by water after entering the PVC tube. The heat transfer in air or water will be addressed in the thermal model.

2.3. Temperature measurements

To measure the temperature of the catheter, seven thermocouples marked by TC1 to TC7 in Figure 2 with 0.36 mm diameter miniature junction tip (5TC-TT-T-36-36, Omega Engineering) were fixed on the outer surface of the sheath using the Teflon tape. The silver thermal paste compound (1978-DP, Techspray) was applied between the thermocouple tip and sheath outside surface to reduce the contact thermal resistance. Thermocouple TC7 was placed at the end of the sheath at a distance L_E from the air turbine ($L_E = 1350$ mm in this study). Thermocouple TC6 was placed on the sheath inside the PVC tube, 200 mm from TC7. Thermocouple TC8 was placed at the exit of sheath to measure the temperature of saline and blood-mimicking water mixture. The distance from the air turbine to TC1 to TC5 are marked in Figure 2(b). The distance from TC7 to the introducer is marked as l, which is one of the vari-

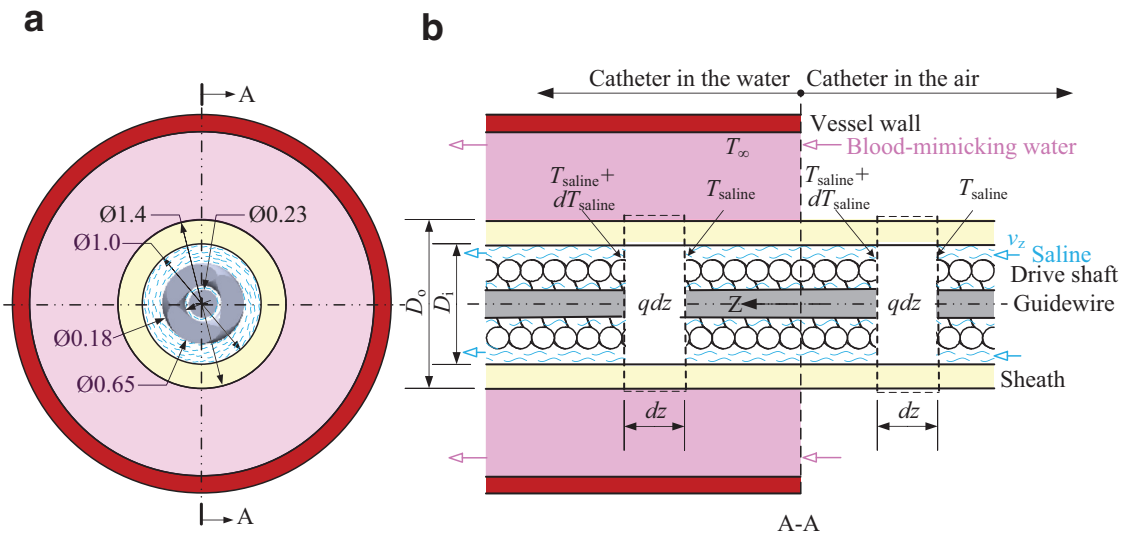

Figure 3. (a) Cross-section view and dimensions of the catheter and (b) control volumes of the thermal model. (Unit: mm).

Table 1
RA procedure parameters and their respective levels in design of experiment.

	Rotational speed, ω (× 1000 rpm)	Blood-mimicking water flow rate, Q_b (ml/min)	Saline flow rate, Q_s (ml/min)	Insertion length, l (m)
Level I	135	40	14	0.3
Lever II	155	20	10	0.5
Level III	175	0	6	0.7

ables in this study. An 8-channel data acquisition system (OMB-DAQ-2408, OMEGA Engineering) was used to record the temperature data at 20 Hz sampling rate. The calibration of the thermocouples was finished before the experiments and uncertainty for the result is ±0.5 °C.

2.4. Experiment design

Four input parameters were investigated: the rotational speed (ω), blood-mimicking water flow rate (Q_b), saline flow rate (Q_s), and insertion length of the sheath inside blood vessel (l). The average blood flow rate was 40 ml/min in the normal popliteal artery [13]. The Q_b was set at 40, 20, and 0 ml/min, representing 0%, 50%, and 100% blockage of the artery, respectively. The pressure of the blood-mimicking water (decided by the height of the reservoir) remains the same. The saline flows at $Q_s = 14$, 10, and 6 ml/min. Three levels of $l = 0.3$, 0.5, and 0.7 m were studied based on the nominal distance of 0.5 m from the femoral artery to the knee popliteal artery for a male subject (178 cm height and 81.2 kg weight). Three levels of parameters in the design of experiment are summarized in Table 1. Based on the L9 (3^4) design of experiment [14], a total of 9 tests, marked from Exps. 1 to 9, were conducted.

3. Thermal model of the catheter

3.1. Thermal model

An advection-diffusion model was developed to predict the spatial and temporal distribution of saline temperature, T_{saline}. The catheter was assumed to have a uniform and stable saline flow. Thermal energy generation q, due to friction between the rotating drive shaft and stationary sheath and guidewire was assumed to be constant with respect to time and location. Temperature variation in the radial direction of the catheter was neglected because the catheter length is much longer than the outer diameter of catheter (1350 vs. 1.4 mm). Temperature was assumed to be axisymmetric. As shown in Figure 3(b), two control volumes with length dz and temperatures T_{saline} and $T_{saline}+dT_{saline}$ at the upstream and downstream side of the control volume, respectively, were used to model the saline temperature. The saline flow has the velocity vector $\mathbf{v}$ and transports the energy in the control volumes. For the control volume in the water, the convective heat transfer coefficient is h. For the control volume in the air, an adiabatic boundary condition was assumed. Based on the conservation of energy [15], the governing equation of this control volume is:

$$\rho c\frac{\partial T_{saline}}{\partial t} - k\nabla^2 T_{saline} + \rho c\mathbf{v}\cdot\nabla T_{saline} = -\frac{4h(T_{saline}-T_\infty)}{D_o} + q \tag{1}$$

where ρ is the saline density, c is the saline specific heat, k is the saline thermal conductivity, t is the RA process time, and T_∞ is the blood-mimicking water temperature. The first-term is the changing rate of the internal energy per unit volume, the second, third, and fourth term is the energy transfer through conduction, advection, and convection, respectively. The last term is the thermal energy generation rate per unit volume.

For the 1D problem as shown in Figure 3(b), $\mathbf{v}$ has a magnitude of v_z, the saline flow speed, $\nabla T_{saline} = \frac{\partial T_{saline}}{\partial z}$, $\nabla^2 T_{saline} = \frac{\partial^2 T_{saline}}{\partial z^2}$, where z is the distance from the starting point of the catheter along its length (as indicated in Fig. 2), the governing equation is simplified to:

$$\frac{\partial T_{saline}}{\partial t} = -v_z\frac{\partial T_{saline}}{\partial z} + K\frac{\partial^2 T_{saline}}{\partial z^2} + Q - H(T_{saline}-T_\infty) \tag{2}$$

where $H = 4h/(\rho c D_o)$, $K = k/(\rho c)$, and $Q = q/(\rho c)$.

Appendix A outlines the solution of Equation (2) for the saline temperature.

$$T_{saline}(z,t) = \sum_{n=1}^{\infty} e^{-(H+K(n\lambda)^2)t}(A_n\sin(n\lambda(z-v_z t)+\varphi_n)) + (b(z-v_z t)+g)e^{-Ht} + \frac{Q}{H} + T_\infty \tag{3}$$

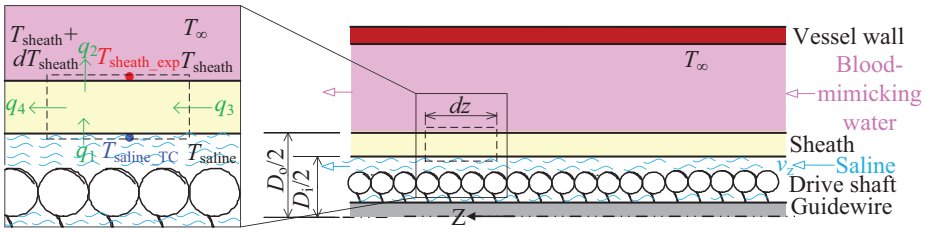

Figure 4. The heat transfer in the control volume of the sheath.

where A_n, φ_n, b, g, and λ are unknown constants, which will be estimated later in the paper.

For the catheter in the air, the initial condition (IC) is $T_{saline}(z, 0) = T_o$, where T_o is the initial saline temperature (constant). The boundary conditions (BCs) are $T_{saline}(0, t) = T_o$ and $T_{saline}(L_I, t) = T_I$, where T_I is the temperature at point I (the point of catheter inserted into the introducer) and L_I is the distance between the catheter starting point and point I, as shown in Figure 2(b). Substituting the IC and BC $T_{saline}(0, t) = T_o$ to Equation (3), Equation (2) is simplified to:

$$T_{saline}(z,t) = \sum_{n=1}^{\infty} e^{-(H+K(n\lambda)^2)t}(A_n \sin(n\lambda(z - v_z t) + \varphi_n)) + b(z - v_z t) + Qt + T_o \quad (4)$$

For the catheter in the water, IC is also $T_{saline}(z, 0) = T_o$. BCs are $T_{saline}(L_I, t) = T_I$ and $T_{saline}(L_E, t) = T_E$, where T_E is the measured temperature from TC7 at point E (the ending point of the catheter) and L_E is the length between the catheter starting point and point E, as shown in Figure 2(b).

3.2. Inverse heat transfer solution

The inverse heat transfer method is applied to solve T_{saline} in two cases using Eqs. (2) and (4). Case 1 is the T_{saline} with catheter in the air and Case 2 is the T_{saline} with catheter in the water. For Case 1, analytical solutions for A_n, φ_n, λ, and b cannot be found due to the unknown BC, T_I. The relationship between Q and rotational speed is also difficult to quantify. For Case 2, Q and H in Equation (2), which change with the rotational speed and blood-mimicking water flow rate, are difficult to determine as well. Values of those unknown constants in both Cases 1 and 2 were solved using the inverse heat transfer analysis by optimizing values of these unknown variables in the thermal model to match the modeling and experimental results.

In Case 1, in order to simplify the series in Equation (4), a sensitivity analysis was first carried out. The difference of the four-term ($n = 1$, 2, 3, and 4) and two-term ($n = 1$ and 2) solutions was less than 1% and a two-term solution was used to model T_{saline} in Equation (4):

$$T_{saline}(z,t) = A_1 \sin(\lambda(z - v_z t) + \varphi_1)e^{-K(\lambda)^2 t} + A_2 \sin(2\lambda(z - v_z t) + \varphi_2)e^{-K(2\lambda)^2 t} + b(z - v_z t) + Qt + T_o \quad (5)$$

where A_1, A_2, φ_1, φ_2, λ, b, and Q are unknown constants to be estimated by the inverse heat transfer solution. The saline speed v_z is calculated by dividing the saline flow rate by the inside cross-section area of the catheter.

For Case 1, the Trust-Region method [12] in the surface fitting toolbox in MATLAB (MathWorks Inc., Natick, MA) is applied to the inverse solution. The lower and upper limits were set as $[-\infty, \infty]$, $[-\infty, \infty]$, $[-\pi, \pi]$, $[-\pi, \pi]$, [0, 2], [0, 30], and [0, 1] for A_1, A_2, φ_1, φ_2, b, Q, and λ, which have the initial values of 0, 0, 0, 0, 0, 1, and 0.1 [16], respectively. The sum of squared errors between the experimental measured and thermal model calculated saline temperatures, E, was minimized to solve those unknown constants in inverse heat transfer solution. When the reduction of E between two consecutive iterations is less than δ, which was set as 10^{-6}, the inverse solution is considered to be convergent. After getting the inverse solution of all constants, T_I and Q can be calculated.

For Case 2, T_{saline} was calculated by the COMSOL Multiphysics 5.2a (Los Angeles, CA) using Equation (2) with two BCs and one IC, as discussed previously. Before the study, the mesh of the catheter was refined until the surface temperature result difference is less than 0.5% through a simple heat conduction process. Values of Q in Equation (2) and T_I from Case 1 were used in Case 2. The MATLAB and COMSOL Multiphysics were linked to solve H using MATLAB's sequential quadratic programming in the nonlinear minimum optimization toolbox. The lower and upper limits of H were [0, 10] and the initial value was 1. E was minimized and the same convergence criterion of Case 1 was used. For both cases, $\rho = 1000\,kg/m^3$, $c = 4719\,J/(kg\cdot K)$, and $k = 0.6\,W/(m\cdot K)$.

3.3. Saline and sheath temperatures

The sheath temperature T_{sheath} was calculated, using T_{saline} as the input and applying the conservation of energy to an axisymmetric control volume of the sheath with length dz and four heat fluxes with surroundings by convection (q_1 and q_2) and conduction (q_3 and q_4), as shown in Figure 4. The temperatures of the sheath on both sides of this control volume are denoted as T_{sheath} and $T_{sheath} + dT_{sheath}$ at z and $z + dz$, respectively. Four heat fluxes are:

$$q_1 = h_s \pi D_i dz(T_{saline} - T_{sheath}) \quad (6)$$

$$q_2 = h\pi D_o dz(T_{sheath} - T_\infty) \quad (7)$$

$$q_3 = -k_s \pi \frac{D_o + D_i}{2} \cdot \frac{D_o - D_i}{2} \cdot \frac{T_{sheath}(z + dz) - T_{sheath}(z)}{dz} \quad (8)$$

$$q_4 = -k_s \pi \frac{D_o + D_i}{2} \cdot \frac{D_o - D_i}{2} \cdot \frac{T_{sheath}(z + dz) - T_{sheath}(z)}{dz} \quad (9)$$

where ρ_s is the density of sheath, c_s is the sheath specific heat, k_s is the sheath thermal conductivity, and h_s is the convective heat transfer coefficient between the saline and sheath. Based on the conservation of energy [15], the governing equation can be written as:

$$q_1 + q_3 - q_2 - q_4 = \rho_s c_s \pi dz \frac{D_o + D_i}{2} \cdot \frac{D_o - D_i}{2} \cdot \frac{\partial T_{sheath}}{\partial t} \quad (10)$$

The computational cell form of Equation (10) can be converted to the differential form:

$$\rho_s c_s \frac{\partial T_{sheath}}{\partial t} - k_s \frac{\partial^2 T_{sheath}}{\partial z^2} = \frac{4h_s D_i (T_{saline} - T_{sheath})}{D_o{}^2 - D_i{}^2} - \frac{4hD_o (T_{sheath} - T_\infty)}{D_o{}^2 - D_i{}^2} \quad (11)$$

The sheath is made of polytetrafluoroethylene with $\rho_s = 2200\,kg/m^3$, $c_s = 1300\,J/(kg\cdot K)$, and $k_s = 0.25\,W/(m\cdot K)$ [17]. The

Table 2
Experimental parameters based on L9 (3^4) design of experiment and measured temperature rise at TC1 to TC8 after 30 s of RA process.
Legend: catheter in the air catheter in the blood-mimicking water

Parameters	Exp. 1	2	3	4	5	6	7	8	9
ω (×1,000 rpm)	135	135	135	155	155	155	175	175	175
Q_b (ml/min)	40	20	0	40	20	0	40	20	0
Q_s (ml/min)	14	10	6	6	14	10	10	6	14
l (m)	0.3	0.5	0.7	0.5	0.7	0.3	0.7	0.3	0.5
TC1 (°C) Mean(SD)	3.2 (0.02)	4.0 (0.01)	6.3 (0.05)	8.3 (0.50)	4.5 (0.04)	5.3 (0.08)	7.3 (0.08)	10.5 (0.15)	6.2 (0.11)
TC2 (°C) Mean(SD)	3.8 (0.04)	5.1 (0.03)	7.3 (0.10)	10.8 (0.33)	5.4 (0.01)	6.1 (0.03)	8.5 (0.01)	12.0 (0.09)	7.6 (0.14)
TC3 (°C) Mean(SD)	4.4 (0.08)	5.5 (0.05)	8.2 (0.16)	12.0 (0.24)	6.6 (0.08)	7.6 (0.01)	9.8 (0.08)	13.2 (0.07)	8.5 (0.14)
TC4 (°C) Mean(SD)	4.9 (0.09)	6.4 (0.07)	4.8 (0.21)	12.5 (0.18)	4.4 (0.24)	7.7 (0.01)	5.0 (0.01)	14.2 (0.07)	10.0 (0.18)
TC5 (°C) Mean(SD)	5.3 (0.01)	3.9 (0.19)	3.1 (0.16)	3.8 (0.23)	3.9 (0.22)	9.1 (0.11)	4.4 (0.12)	15.6 (0.22)	6.0 (0.15)
TC6 (°C) Mean(SD)	2.8 (0.15)	2.9 (0.26)	2.3 (0.18)	3.4 (0.37)	3.0 (0.14)	4.9 (0.27)	4.0 (0.17)	7.4 (0.33)	4.5 (0.12)
TC7 (°C) Mean(SD)	2.6 (0.05)	3.5 (0.27)	3.6 (0.28)	3.2 (0.22)	4.0 (0.26)	6.4 (0.25)	5.0 (0.35)	5.1 (0.48)	8.3 (0.33)
TC8 (°C) Mean(SD)	3.4 (0.04)	3.8 (0.15)	3.9 (0.35)	3.9 (0.16)	4.3 (0.32)	7.4 (0.24)	5.8 (0.3)	7.2 (0.62)	8.9 (0.34)

saline flow was assumed fully developed due to the small thermal entry length, $L_{TE} = 0.05 ReD_i Pr$ [15], where Re is the Reynold's number (=510 for 14 mL/min saline flow rate), and Pr is the Prandtl number (=6.62 for water at 22 °C). L_{TE} is calculated to be 0.17 m and is much small than the total length of the sheath 1.35 m. By assuming a uniform heat flux, $h_s = 4.36 k_s / D_i = 1090\ \mathrm{W/(m^2 \cdot K)}$ [15].

Equation (11) was solved numerically using MATLAB with forwarding time and central space scheme to calculate T_{sheath}. The calculated the T_{sheath} was compared with T_{sheath_exp} measured in the experiments to guide an iterative solution to find T_{saline}. The detail of the iterative solution for T_{saline} calculation is shown in Appendix B.

4. Results and discussion

4.1. Experiment temperature and effects of RA operating parameters

The temperature rises of sheath and blood-mimicking water mixture measured by TC1 to TC8 after 30 s of RA were listed in Table 2. For three experiments with $\omega = 135{,}000$ rpm (Exps. 1, 2, and 3), the temperature rise of TC8 (at the outlet of sheath) were all below 4 °C, indicating RA is safe in terms of thermal damage (assuming 6 °C temperature rise is the thermal damage threshold [4–6]). When the ω increased to 155,000 rpm, the temperature rise at TC8 was higher. The temperature rise of 7.4 °C (higher than the 6 °C) was found in Exp. 6 in an occluded artery ($Q_b = 0$) due to less convective heat transfer to the blood-mimicking water. As the ω further increases to 175,000 rpm, all three experiments (Exps. 7 – 9) had temperature rise higher than 6 °C. Exp. 9 showed the highest temperature rise at TC8 (8.9 °C) due to the combination of high ω and low Q_b (= 0).

Figure 5 is a comprehensive summary of experimentally measured sheath temperature rise ΔT_{s_exp} ($=T_{sheath\_exp} - T_\infty$), representing in solid lines, at TC1, TC3, TC5, and TC7 during the 30 s of RA. Key observations are:

Exp. 1 results: Exp. 1 has the lowest ω (135,000 rpm), the highest Q_s (14 ml/min) and Q_b (40 ml/min), and the shortest l (0.3 m). Results in Exp. 1 in Figure 5(a) have the minimum ΔT_{s_exp} for both catheters in air and in blood-mimicking water. The ΔT_{s_exp} increased in the first 15 s for the catheter in the air (TC1, TC3, and TC5), which indicates a steady thermal energy generation inside the catheter. After 15 s, ΔT_{s_exp} reaches a steady state of 3.2, 4.4, and 5.3 °C at TC1, TC3, and TC5, respectively. Due to the steady thermal energy generation inside the catheter, higher sheath temperature rise (at TC5) was observed farther away from the air turbine. The ΔT_{s_exp} of TC7 at $t = 30$ s (marked by the pink circle in Fig. 5) is 2.6 °C, much lower than that of TC1, TC3, and TC5 (in the air) due to the cooling by the blood-mimicking water.

Effects of process time and catheter length and cooling after entering the introducer: In the other 8 experiments, a similar trend of ΔT_{s_exp} which increase with the time and distance from the air turbine and slightly drops after the catheter entered the blooding-mimicking water has been observed.

Effect of wheel rotational speed: The high ω (175,000 rpm) significantly elevates the ΔT_{s_exp} when the Q_s is low (6 ml/min) in Exp. 8 or the Q_b is low (0 ml/min) in Exp. 9. In Exp. 8, the ΔT_{s_exp} in TC1 – TC5 increases rapidly due to high thermal energy generation rate inside catheter.

Effect of blood-mimicking water flow rate on TC7 temperature: The high Q_b (40 ml/min) helps to lower ΔT_{s_exp} in RA. In Exp. 9, at $Q_b = 0$ ml/min, the ΔT_{s_exp} at TC7 steadily increase over time to 8.3 °C (the highest among all experiments) without much cooling with the catheter in the air and in the PVC tube with nonflowing blood-mimicking water.

Statistical analysis of significance of TC7 and TC8: In the design of experiment, analysis of variance (ANOVA) is applied to study the significance of four parameters ω, Q_b, Q_s, and l [18]. Table 3 shows the ANOVA of ΔT_{s_exp} at TC7 and TC8. At TC8, which is the most

Table 3
ANOVA results of TC7 and TC8 (DOF = 2).

Input Parameter	p-value TC7	TC8
ω	0.072	0.037
Q_b	0.088	0.078
Q_s	0.329	0.5
L	0.5	0.213

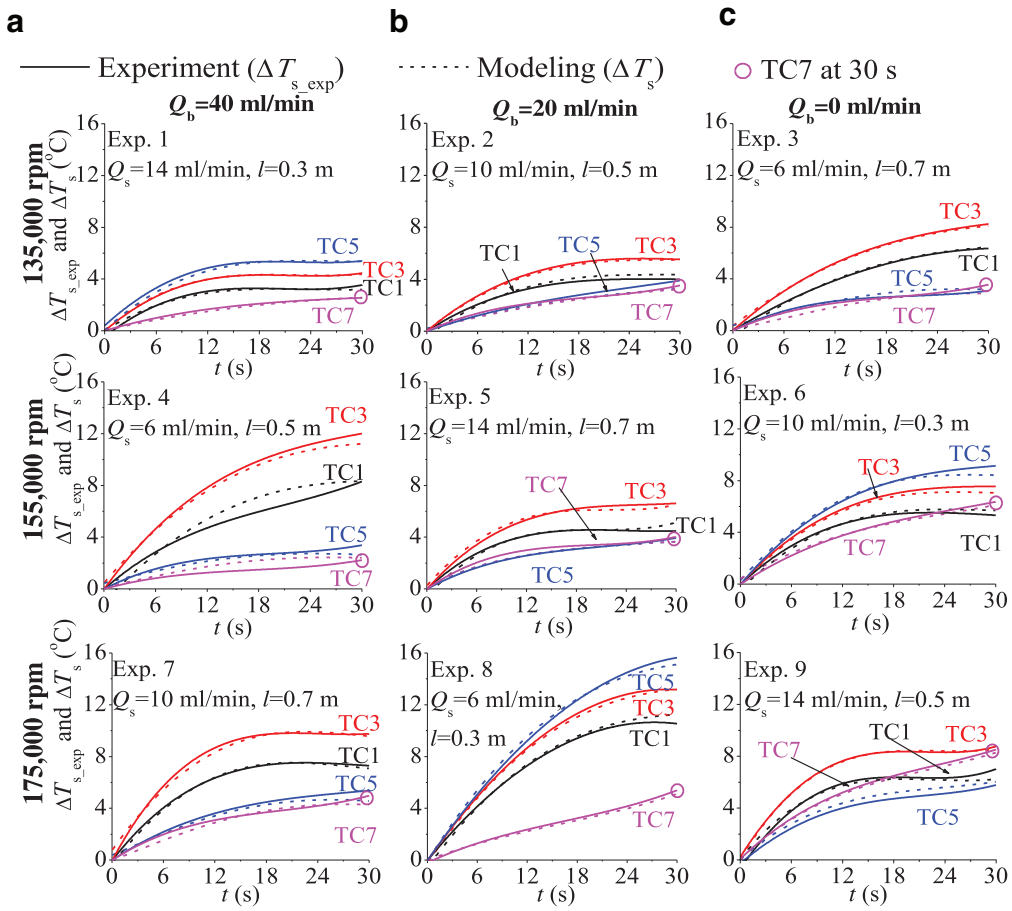

Figure 5. Experimentally measured and model predicted temperature rise for blood-mimicking water flow rate in (a) 40, (b) 20, and (c) 0 ml/min.

important indicator clinically, ω is the most significant factor with $p = 0.037$. Q_b also has a significant effect with $p = 0.078$. The effect of l and Q_s is not as significant, as evident in the observations shown in Figure 5. Similarly, at TC7, ω and Q_b also have significant effects with $p = 0.072$ and 0.088, respectively.

From the results above, a totally occluded lesion ($Q_b = 0$) with no blood flow combined with high grinding wheel rotational speed can lead to excessive temperature rise and may cause blood coagulation in RA. The potential ways to reduce the temperature rise in RA are using lower rotational speed and higher saline flow rate.

4.2. Modeling results

The thermal energy generation rate q and convective heat transfer coefficient h, which were calculated by the Q and H from the inverse heat transfer solution and using $q = \rho c Q$ and $h = \rho c D_0 h/4$, are listed in Table 2. Values of q are similar for the same rotational speed (Exps. 1, 2, and 3; Exps. 4, 5, and 6; Exps. 7, 8, and 9) and increase with the rotational speed. The values of h vary from 3312 to 9224 W/(m^2·K).

Figure 5 also shows model predicted temperature rise at TC1, TC3, TC5, and TC7, using the thermal model and parameters (q, h, A_1, φ_1, A_2, φ_2, b, λ) from the inverse heat transfer solution listed in Appendix C. The model predicted temperature rise ΔT_s ($= T_{sheath} - T_\infty$) matches well with experimentally measured results and indicates the potential for accurate prediction of saline temperature, which is difficult to measure. Table 4 also gives the coefficient of determination (R^2) to evaluate the agreement between the model prediction and the experimental measurement results.

Table 4
Inverse heat transfer solution and coefficient of determination (R^2).

Exp. #	q ($\times$ 10^6 W/m^3)	h ($\times$ 10^3 W/(m^2·K))	R^2
1	4.49	7.85	0.98
2	4.33	4.35	0.95
3	4.35	2.65	0.87
4	7.33	9.22	0.90
5	6.65	4.66	0.93
6	6.36	7.04	0.99
7	7.92	4.01	0.94
8	8.04	3.31	0.95
9	8.59	6.16	0.93

$$R^2 = 1 - \sum_{j=1}^{7} \left({}^jT_{sheath} - {}^jT_{sheath\_exp}\right)^2 / \sum_{j=1}^{7} \left({}^j\overline{T}_{sheath\_exp} - {}^jT_{sheath\_exp}\right)^2 \quad (12)$$

where $\overline{T}_{sheath\_exp}$ is the mean of experimentally measured temperature.

All R^2 are larger than 0.90 except Exp. 3. This shows a good fidelity of the thermal model.

Figure 6 shows the comparison between the experimental and modeling results of the saline temperature rise at TC8 in Exps. 1 (lowest temperature in blood-mimicking water and air), 8 (highest temperature in the air), and 9 (highest temperature in blood-mimicking water). The measured temperature rise ΔT_{exp} is $T_{exp\_TC8} - T_\infty$, where T_{exp_TC8} is the measured saline and blood-mimicking water mixture temperature at TC8 (the outlet of the sheath), and ΔT is calculated by ${}^8T_{saline} - T_\infty$, where ${}^8T_{saline}$ is the

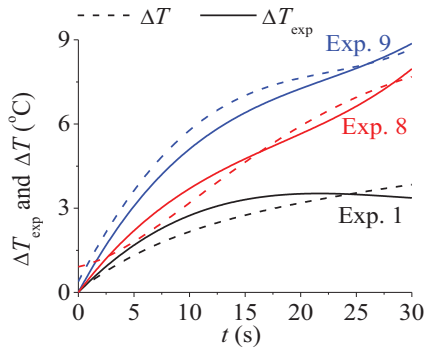

Figure 6. Experiment measured and model predicted saline temperature rise at TC8 (outlet of the catheter).

thermal model predicted saline temperature at TC8 location. The discrepancy between modeling and experimental saline temperature results is likely due to the thermocouple tip vibration in the flowing saline, which affects the measurement process and result accuracy. For Exps. 1, 8, and 9 in Figure 6, the R^2 is calculated by $1-\sum_{i=1}^{600}\left({}^{i}\Delta T-{}^{i}\Delta T_{\exp}\right)^2/\sum_{i=1}^{600}\left(\overline{\Delta T}_{\exp}-{}^{i}\Delta T_{\exp}\right)^2$, where i is the index number (=1, 8, or 9). The value of R^2 is 0.93, 0.96, and 0.97 for Exps. 1, 8, and 9, respectively. This good match proved the correctness of our thermal model and the iterative solution.

5. Clinical relevance

Thermal damage may occur during RA at high rotational speed and low blood flow rate, based on the experiment and modeling results. To avoid thermal damage, the slow rotational speed (lower than 155,000 rpm) with high saline flow rate (higher than 18 ml/min) are recommended to decrease the thermal energy generation rate and increase the advection, during the RA in severely occluded lesions. In addition, from the thermal model prediction, pre-cooling the saline to 15 °C can potentially reduce the blood thermal damage in RA. For RA device design, a low friction coefficient material for drive shaft and guidewire should be considered to reduce the friction thermal energy generation.

6. Conclusions

The thermal model together with the inverse heat transfer method had demonstrated to be capable to predict the spatial and temporal temperature distributions of catheter in RA procedure. The wheel rotational speed and blood flow rate were identified as the two most critical factors on the temperature of the blood and saline mixture. The level of occlusion of the artery greatly affected the catheter temperature rise in RA. The combination of 175,000 rpm wheel rotational speed and several vessel occlusion conditions in RA with normal saline flow rate (about 10 ml/min) caused the blood-mimicking water temperature to rise more than 9 °C, which might induce potential blood coagulation and corresponding slow-flow/no-reflow and myocardial infarction complications.

The thermal model developed to predict the saline temperature has a reasonably good correlation on the model-predicted and experimentally-measured sheath temperatures. Optimizing the saline temperature for minimum temperature rise at the grinding site is an obvious next-step in this research. The other on-going research is to further establish clinical guidelines on the wheel speed and saline flow rate based on the level of occlusion (blood flow rate). In addition to the blood temperature, the grinding wheel speed also affects the debris particle size, which is also clinically important. A low wheel speed can reduce the temperature but will increase the debris particle size.

Acknowledgement

The authors are grateful for the financial support from the National Natural Science Foundation of China, NSFC), (Grant no. 51705479).

Conflict of interest

None declared.

Funding

None.

Appendix A. Solution of the saline temperature

From Equation (2), denote $\theta = T_{\text{saline}} - T_\infty$,

$$\frac{\partial\theta}{\partial t} = -v_z\frac{\partial\theta}{\partial z} + K\frac{\partial^2\theta}{\partial z^2} + Q - H\theta \tag{A1}$$

Assume $\theta(z, t) = u(z - v_z t, t)$,

$$\frac{\partial\theta}{\partial t} = -v_z\frac{\partial u}{\partial z} + \frac{\partial u}{\partial t} \tag{A2}$$

Substitute Equation (A2) to Equation (A1),

$$\frac{\partial u}{\partial t} = K\frac{\partial^2 u}{\partial z^2} + Q - Hu \tag{A3}$$

Set $u = v + w$, where v is the solution for the homogeneous equation: $\frac{dv}{dt} = K\frac{d^2v}{dz^2} - Hv$ and $w = Q/H$ is the solution for the inhomogeneous part.

To solve v, the separation of variable is applied:

$$v(z, t) = Z(z)T(t) \tag{A4}$$

The equation $\frac{\partial v}{\partial t} = K\frac{\partial^2 v}{\partial z^2} + Q$ can be converted to:

$$\frac{T'}{KT} + \frac{H}{K} = \frac{Z''}{Z} = -(n\lambda)^2 \tag{A5}$$

where $n = 1, 2, 3, \ldots$

When $n\lambda = 0, v = e^{-Ht}(bz + g)$, where b and g are constants.

When $n\lambda \neq 0$,

$$v = \sum_{n=1}^{\infty} e^{-(H+K(n\lambda)^2)t}\left(A_n \sin(n\lambda z + \varphi_n)\right) \tag{A6}$$

where A_n and φ_n are constants.

Combing the solutions of v and w:

$$u(z, t) = \sum_{n=1}^{\infty} e^{-(H+K(n\lambda)^2)t}\left(A_n \sin(n\lambda z + \varphi_n)\right) + (bz + g)e^{-Ht} + \frac{Q}{H} \tag{A7}$$

Converting the variable from $u(z, t)$ to $T_{\text{saline}}(z, t)$, the solution of Equation (A3) is

$$T_{\text{saline}}(z, t) = \sum_{n=1}^{\infty} e^{-(H+K(n\lambda)^2)t}\left(A_n \sin(n\lambda(z - v_z t) + \varphi_n)\right) + (b(z - v_z t) + g)e^{-Ht} + \frac{Q}{H} + T_\infty \tag{A8}$$

For the catheter in the air, applying BC $T_{\text{saline}}(0, t) = T_o$ and IC $T_{\text{saline}}(z, 0) = T_o$, $g = T_o - T_\infty - Q/H$, Equation (A8) converts to

$$T_{\text{saline}}(z, t) = \sum_{n=1}^{\infty} e^{-(H+K(n\lambda)^2)t}\left(A_n \sin(n\lambda(z - v_z t) + \varphi_n)\right) + b(z - v_z t)e^{-Ht} + \frac{Q}{H}(1 - e^{-Ht}) + (T_o - T_\infty)e^{-Ht} + T_\infty \tag{A9}$$

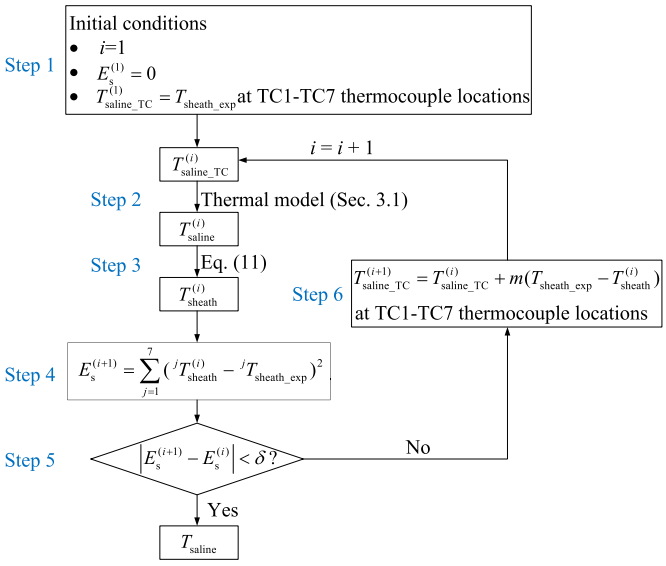

Figure B1. Flow chart for saline temperature iterative solution.

The heat convection to the air is assumed to be negligible, $h=0$ and $H=0$. The Taylor series for e^{-Ht} at $H=0$ is $\frac{(-Ht)^0}{0!} + \frac{(-Ht)^1}{1!} + \frac{(-Ht)^2}{2!} + \frac{(-Ht)^3}{3!} + \frac{(-Ht)^4}{4!} + \cdots$). The third term in Equation (A9) is $Q(t - \frac{Ht^2}{2!} + \frac{H^2t^3}{3!} - \cdots)$. The solution for the catheter in the air converts to:

$$T_{saline}(z,t) = \sum_{n=1}^{\infty} e^{-(H+K(n\lambda)^2)t}(A_n \sin(n\lambda(z - v_z t) + \varphi_n)) + b(z - v_z t) + Qt + T_o \quad \text{(A10)}$$

Appendix B. Iterative solution of the saline temperature

The iterative solution to find T_{saline} using T_{sheath_exp} as input is based on the following six steps, as shown in Figure B1.

Step 1. Initial conditions: The iteration index number i, denoted as the right superscript, is set as 1. The sum of squared errors between $T_{sheath}^{(i)}$ and T_{sheath_exp} at TC1-TC7 thermocouple locations, denoted as $E_s^{(i)}$, has an initial value of 0. The initial saline temperature $T_{saline\_TC}^{(1)}$ at TC1-TC7 thermocouple locations are the same with T_{sheath_exp} at the same locations.

Step 2. Thermal model solution in iteration i: $T_{saline\_TC}^{(i)}$ is used to calculate the temporal and spatial distribution of saline temperature along the entire catheter $T_{saline}^{(i)}$ by the thermal model described in Section 3.1.

Step 3. Sheath temperature solution: $T_{saline}^{(i)}$ is used to calculate the temporal and spatial distribution of sheath temperature along the entire catheter $T_{sheath}^{(i)}$ using Equation (11), which cannot be solved due to the lack of BCs. To solve $T_{sheath}^{(i)}$, the left-hand side of Equation (11) is simplified by assuming $\frac{\partial T_{sheath}^{(i)}}{\partial t} = \frac{\partial T_{sheath}^{(i-1)}}{\partial t}$, $\frac{\partial^2 T_{sheath}^{(i)}}{\partial z^2} = \frac{\partial^2 T_{sheath}^{(i-1)}}{\partial t^2}$ and $\frac{\partial T_{sheath}^{(1)}}{\partial t} = \frac{\partial T_{saline}^{(1)}}{\partial t}$, $\frac{\partial^2 T_{sheath}^{(1)}}{\partial z^2} = \frac{\partial^2 T_{saline}^{(1)}}{\partial z^2}$.

Step 4. Error calculation: The difference between $T_{sheath}^{(i)}$ and T_{sheath_exp} at TC1-TC7 thermocouple locations is evaluated by calculating the sum of squared errors, $E_s^{(i+1)} = \sum_{j=1}^{7} ({}^{j}T_{sheath}^{(i+1)} - {}^{j}T_{sheath\_exp})^2$, where j is the thermocouple index number, denoted as the left superscript.

Step 5. Convergence check: The difference of E_s between two consecutive iterations is calculated. If the difference is smaller than δ, which was set as 10^{-6} in this study, the iteration is considered convergent and the output $T_{sheath} = T_{sheath}^{(i)}$. Otherwise, Step 6 is executed and the iteration continues.

Step 6. Update of saline temperature at thermocouple locations: Errors between T_{sheath_exp} and $T_{sheath}^{(i)}$ at TC1-TC7 thermocouple locations are applied to update $T_{saline\_TC}^{(i)}$. The value of saline temperature in the next $(i+1)$-th iteration $T_{saline\_TC}^{(i+1)}$ is predicted using $T_{saline\_TC}^{(i)} + m(T_{sheath\_exp} - T_{sheath}^{(i)})$, where m is a constant to adjust the convergence. The m for the minimum number of iterations is evaluated based on the experimental results. For the theoretical minimum number of iterations, which is $i=2$, the iterative result at TC7 location (point E in Fig. 2(b)) can be expressed as $T_{exp\_TC8} = T_{exp\_TC7} + m(T_{exp\_TC7} - T_{sheath}^{(1)})$, where T_{exp_TC8} and T_{exp_TC7} are the saline and sheath temperature measured by TC8 and TC7 in the experiments. Assuming a linear relationship between the T_{saline} and T_{sheath}, the $T_{sheath}^{(1)}$ can be replaced by $T_{sheath}/T_{saline} \cdot T_{saline}^{(1)}$ and m is calculated as T_{exp_TC8}/T_{exp_TC7}. A test was conducted to evaluate the value of m on convergence in Exp. 7, in which T_{exp_TC8}/T_{exp_TC7}=1.12. For $m=0.9$, 1.0, 1.12, and 1.2, the number of iterations was 15, 13, 12, and 15, respectively. Regardless of the value of m, the T_{saline} solution remained the same, indicating that m does not affect the convergence result.

Table C1
Inverse heat transfer solution.

Exp. #	A_1	φ_1	A_2	φ_2	b	λ
1	27.8	−1.88	−28.0	−1.96	0.38	0.062
2	31.5	−1.73	−32.8	−1.94	0.00	0.069
3	43.3	−0.96	−35.1	−1.71	0.00	0.080
4	70.9	−1.72	−77.4	−2.06	0.00	0.031
5	35.0	−0.92	−27.5	−1.72	0.29	0.055
6	49.4	−2.05	−47.6	−2.00	0.01	0.071
7	58.4	−2.15	−56.5	−2.14	0.00	0.077
8	80.7	−1.25	−88.2	−0.95	4.54	0.030
9	48.4	−1.73	−50.1	−1.94	0.60	0.062

Appendix C. Results of inverse heat transfer solution

The solution of A_1, φ_1, A_2, φ_2, b, and λ for Exps. 1 to 9 is summarized in Table C1.

References

[1] Tomey MI, Kini AS, Sharma SK. Current status of rotational atherectomy. JACC Cardiovasc Interv 2014;7(4):345–53.
[2] Fitzgerald P, Ports T, Yock P. Contribution of localized calcium deposits to dissections after angioplasty. Circulation 1992;86(1):64–70.
[3] Barbato E, Carrié D, Dardas P, Fajadet J, Gaul G, Haude M, Khashaba A, Koch K, Meyer-Gessner M, Palazuelos J, Reczuch K, Ribichini FL, Sharma S, Sipötz J, Sjögren I, Suetsch G, Szabó G, Valdés-Chávarri M, Vaquerizo B, Wijns W, Windecker S, de Belder A. European expert consensus on rotational atherectomy. Euro Interv 2015;11(1):30–6.
[4] Gader AMA, Al-Mashhadani SA, Al-Harthy SS. Direct activation of platelets by heat is the possible trigger of the coagulopathy of heat stroke. British J Haentalog 1990;74:86–92.
[5] White JG. Effects of heat on platelet structure and function. Blood 1968;32(2):324–35.
[6] Rao GH, Smith CM, Escolar G, White JG. Influence of heat on platelet biochemistry, structure, and function. J Lab Clin Med 1993;122(4):455–64.
[7] Cavusoglu E, Kini AS, Marmur JD, Sharma SK. Current status of rotational atherectomy. Catheter Cardiovasc Interv 2004;62(4):485–98.
[8] Morii I, Miyazaki S. Current overview of rotational atherectomy. Does rotablator make sense. Emodinamica 2000;22:2–9.
[9] Abdurrazzak A, Gehani MRR. Can rotational atherectomy cause thermal tissue damage a study of the potential heating and thermal tissue effects of a rotational atherectomy device. Cardiovasc Intervent Radiol 1998;21:481–6.

[10] Reisman M, Shuman BJ, Harms V. Analysis of heat generation during rotational atherectomy using different operational techniques. Cathet Cardiovasc Diagn 1998;44(4):453–5.
[11] Shih AJ, Liu Y, Zheng Y. Grinding wheel motion, force, temperature, and material removal in rotational atherectomy of calcified plaque. CIRP Annals - Manuf Technol 2016;65:345–8.
[12] Tai BL, Stephenson DA, Shih AJ. An inverse heat transfer method for determining workpiece temperature in minimum quantity lubrication deep hole drilling. J Manuf Sci Eng 2012;134:1–7.
[13] Ramazani-Rend R, Chelikani S, Sparrow EM, Abraham JP. Experimental and numerical investigation of orbital atherectomy: absence of cavitation. J Biomed Sci Eng 2010;03(11):1108–16.
[14] Sharma P, Verma A, Sidhu RK, Pandey OP. Process parameter selection for strontium ferrite sintered magnets using Taguchi L9 orthogonal design. J Mater Process Technol 2005;168(1):147–51.
[15] Incropera FR, Dewitt DP, Bergman TL, Lavine AS. Introduction to heat transfer. John Wiley & Sons 2007.
[16] Wu C, Pang J, Li B, Liang SY. High-speed grinding of HIP-SiC ceramics on transformation of microscopic features. Int J Adv Manuf Technol 2019;102:1913–21. doi:10.1007/s00170-018-03226-4.
[17] DuPont. Teflon PTFE properties handbook; 2017 http://www.rjchase.com/ptfe_handbook.pdf.
[18] Taguchi G. Introduction to quality engineering: designing quality into products and processes, Asian Productivity Organization, 1986.